Transient Climate Response in a Two-Layer Energy-Balance Model. Part I: Analytical Solution and Parameter Calibration Using CMIP5 AOGCM Experiments

O. GEOFFROY AND D. SAINT-MARTIN

Centre National de Recherches Météorologiques, Groupe d'études de l'Atmosphère Météorologique (CNRM-GAME), Toulouse, France

D. J. L. OLIVIÉ

Center for International Climate and Environmental Research–Oslo, and University of Oslo, Oslo, Norway

A. VOLDOIRE, G. BELLON, AND S. TYTÉCA

Centre National de Recherches Météorologiques, Groupe d'études de l'Atmosphère Météorologique (CNRM-GAME), Toulouse, France

ABSTRACT

This is the first part of a series of two articles analyzing the global thermal properties of atmosphere–ocean coupled general circulation models (AOGCMs) within the framework of a two-layer energy-balance model (EBM). In this part, the general analytical solution of the system is given and two idealized climate change scenarios, one with a step forcing and one with a linear forcing, are discussed. These solutions give a didactic description of the contributions from the equilibrium response and of the fast and slow transient responses during a climate transition. Based on these analytical solutions, a simple and physically based procedure to calibrate the two-layer model parameters using an AOGCM step-forcing experiment is introduced. Using this procedure, the global thermal properties of 16 AOGCMs participating in phase 5 of the Coupled Model Intercomparison Project (CMIP5) are determined. It is shown that, for a given AOGCM, the EBM tuned with only the abrupt $4\times CO_2$ experiment is able to reproduce with a very good accuracy the temperature evolution in both a step-forcing and a linear-forcing experiment. The role of the upper-ocean and deep-ocean heat uptakes in the fast and slow responses is also discussed. One of the main weaknesses of the simple EBM discussed in this part is its ability to represent the evolution of the top-of-the-atmosphere radiative imbalance in the transient regime. This issue is addressed in Part II by taking into account the efficacy factor of deep-ocean heat uptake.

1. Introduction

Determining the response of the climate system to an imposed external perturbation is a major challenge in climate science. The global and annual mean surface temperature response is a useful metric to determine the magnitude of a climate change induced by an externally imposed radiative perturbation. Indeed, many studies suggest that most of the climate variables are related to the global mean surface temperature response. Coupled atmosphere–ocean general circulation models (AOGCMs) are the most comprehensive tool to study climate changes and perform climate projections. They can be used to assess the changes in global temperature but they are computationally expensive. Alternatively, simple climate models (SCMs), which estimate approximately the global mean surface temperature change for a given externally imposed perturbation in the earth's radiation balance (Meinshausen et al. 2011; Good et al. 2011; Friend 2011; van Hateren 2013), can be used to emulate the AOGCM responses in order to cover a wide range of scenarios at a negligible computational cost.

Energy-balance models (EBMs) are physically based SCMs. They are useful to summarize AOGCM global thermal properties and to compare and analyze AOGCM

Corresponding author address: Olivier Geoffroy, Centre National de Recherches Météorologiques (CNRM-GAME), 42 av. G. Coriolis, 31057 Toulouse, France.
E-mail: olivier.geoffroy@meteo.fr

responses (Raper et al. 2002; Soden and Held 2006; Gregory and Forster 2008; Dufresne and Bony 2008). In the case of a small perturbation, some EBMs assume that the thermal energy balance of the climate system is only expressed as a linear function of temperature perturbation (Budyko 1969; Sellers 1969). The net radiative imbalance caused by an external forcing and a temperature change can be expressed as $N = \mathcal{F} - \lambda T$. The radiative feedback parameter λ with respect to the global mean surface air temperature T depends on the type of forcing (Hansen et al. 2005). The imposed radiative forcing $\mathcal{F}$ includes the effects of fast (few months) stratospheric and tropospheric adjustments (Gregory and Webb 2008). In this formulation of the radiative imbalance N, the assumption of linear dependency in T suffers from some limitations (Gregory et al. 2004; Williams et al. 2008; Winton et al. 2010; Held et al. 2010) that are addressed in Part II of this study (Geoffroy et al. 2013, hereafter Part II).

In equilibrium, $N = 0$ and the steady-state temperature is equal to $T_{eq} = \mathcal{F}/\lambda$. Equilibrium climate sensitivity (ECS), which is defined as the equilibrium mean surface air temperature perturbation resulting from a doubling carbon dioxide radiative forcing, is commonly used as a metric of anthropogenic climate change. However, this metric is not sufficient to study the transient regime because of the climate system's thermal inertia. Indeed, the rate of change in the heat content of the climate system is equal to the earth's radiative imbalance and this change occurs on large time scales because of the large thermal inertia of the deep ocean (Dickinson 1981; Hasselmann et al. 1993; Murphy 1995; Gregory 2000; Held et al. 2010). Based on empirical relationships, Gregory and Mitchell (1997) and Raper et al. (2002) propose a formulation for the deep-ocean heat uptake, which is proportional to the surface temperature perturbation, $H = \kappa T$. However, this formulation is not able to represent the equilibrium temperature response in the case of a step-forcing or a stabilization scenario because the deep-ocean temperature response is by definition neglected.

The solution to circumvent this shortcoming is to introduce a second layer that represents the deep ocean. Splitting of the climate system into two thermal reservoirs with different heat capacities allows one to account for the ocean thermal saturation along a transient regime until equilibrium and to represent the two distinct time scales of the global mean climate system response (Hasselmann et al. 1993; Held et al. 2010). This system is similar to the three-layer EBM presented in Dickinson (1981), the atmosphere and the upper-ocean layers being considered as one single layer characterized by the surface air temperature.

In this study, we derive the analytical solution of this two-layer energy-balance model and propose a calibration method to determine the equivalent thermal parameters of a given AOGCM. We then assess the validity of this simple framework to represent the behavior of the complex coupled models in response to an idealized forcing scenario by analyzing the results of 16 AOGCMs participating in the fifth phase of the Coupled Model Intercomparison Project (CMIP5). The role of each layer's heat uptake in the fast and slow components of the transient response is also discussed.

The structure of the paper is as follows: after introducing the theoretical framework and describing the analytical solutions for different forcing scenarios in section 2, the methodology used to adjust the two-layer EBM response to AOGCMs results is presented and applied to CMIP5 AOGCMs in section 3.

2. Theoretical framework

a. Two-layer energy-balance model

We consider the linear two-layer energy-balance model described in Held et al. (2010). Held et al. (2010) also proposed an alternative model with an additional parameter, an efficacy factor for deep-ocean heat uptake, which will be discussed in Part II. The climate system is split into two layers (Gregory and Mitchell 1997; Gregory 2000). The first one corresponds to the atmosphere, the land surface, and the upper ocean, and the second one represents the deep ocean. The state of each layer is described by the temperature perturbations T and T_0. Note that T is usually taken as the global mean surface air temperature perturbation from the control climate, while T_0 is a characteristic temperature perturbation of the deep ocean. Here, T and T_0 satisfy the following system of equations:

$$C\frac{dT}{dt} = \mathcal{F} - \lambda T - \gamma(T - T_0) \quad \text{and} \quad (1)$$

$$C_0\frac{dT_0}{dt} = \gamma(T - T_0). \quad (2)$$

This system has two prognostic variables T and T_0 and five free parameters: λ, γ, C, C_0, and a radiative forcing amplitude parameter $\mathcal{F}$. Whatever the radiative forcing agent, the radiative forcing formulation requires at least one model-dependent reference radiative parameter $\mathcal{F}_{ref}$ caused by stratospheric and tropospheric adjustments. In the case of a CO_2 perturbation, the radiative forcing can be expressed as a function of the CO_2 concentration and a radiative parameter following (Houghton et al. 1990)

$$\mathcal{F}(t) = \frac{\mathcal{F}_{2\times CO_2}}{\ln(2)} \ln\left(\frac{[CO_2]_t}{[CO_2]_0}\right), \qquad (3)$$

where $[CO_2]_t$ is the time-dependent carbon dioxide concentration, $[CO_2]_0$ is the preindustrial CO_2 concentration, and $\mathcal{F}_{2\times CO_2}$ is the net radiative forcing associated with a doubling of the atmospheric CO_2 concentration.

Here $C(dT/dt)$ and $C_0(dT_0/dt)$ are the tendencies of heat contents respectively of the upper and the lower layer; C and C_0 are effective heat capacities (per unit area) of the upper ocean (we neglect the heat capacities of the atmosphere and land surfaces) and the deep ocean, respectively. The parameter γ is a heat exchange coefficient. The heat flux exchange between the two layers is thus assumed to be proportional to the difference between the two temperature perturbations. In the limit of an infinite deep-ocean heat capacity $C_0 \to \infty$, T_0 is zero and the expression of the heat flux exchange is the one proposed by Gregory and Mitchell (1997) with $\kappa = \gamma$. In this one-layer model (the deep-ocean layer is an external infinite reservoir), the temperature perturbation follows the equation

$$C\frac{dT}{dt} = \mathcal{F} - \lambda T - \kappa T. \qquad (4)$$

Such systems can be advantageously described in terms of equivalent electrical circuits (Schwartz 2008; van Hateren 2013). In appendix B, the equivalent electrical circuits of the one- and two-layer EBMs are presented and differences are discussed. A main difference between the one- and two-layer EBM is that the one-layer EBM does not allow the equilibrium temperature to be reached. Indeed, the temperature response in equilibrium is equal to $\mathcal{F}/(\lambda + \kappa)$. The zero-layer EBM [$C = 0$ in Eq. (4)] is an approximate version of the one-layer EBM commonly used (Raper et al. 2002; Dufresne and Bony 2008). Such a model does not allow the representation of the transition for step-forcing cases because the temperature response is a linear function of the forcing. Finally, the zero- and one-layer EBM are per definition not able to represent all kinds of climate change scenarios.

The temperature T_H associated with the climate-system heat uptake is defined as the disequilibrium temperature difference between T and the instantaneous equilibrium temperature $T_{eq}(t) = \mathcal{F}(t)/\lambda$ (Winton et al. 2010). The latter is the equilibrium temperature associated with the instantaneous forcing applied at time t. The heat-uptake temperature represents the instantaneous rate of heat storage in the climate system and follows the equation

$$T_H(t) = T(t) - T_{eq}(t) = -\frac{1}{\lambda}\left(C\frac{dT}{dt} + C_0\frac{dT_0}{dt}\right). \qquad (5)$$

Contrary to Winton et al. (2010), a negative heat-uptake temperature corresponds here to a positive heat storage in the climate system.

b. Analytical solutions

In appendix B, the general solutions of both the mean surface temperature and the deep-ocean temperature responses are derived for any forcing function $t \to \mathcal{F}(t)$. With an integration by parts of Eqs. (B8) and (B9), the temperature perturbations T and T_0 can be written as the sum of the balanced temperature $T_{eq}(t)$ and two modes characterized by two distinct time scales, τ_f (fast) and τ_s (slow), as follows:

$$T(t) = T_{eq}(t) - \sum_{i=\{s,f\}} \frac{a_i}{\lambda}\left[\mathcal{F}(0)e^{-t/\tau_i}\right.$$
$$\left. + \int_0^t \mathcal{F}'(\xi)e^{-(t-\xi)/\tau_i}\,d\xi\right] \quad \text{and} \qquad (6)$$

$$T_0(t) = T_{eq}(t) - \sum_{i=\{s,f\}} \frac{\phi_i a_i}{\lambda}\left[\mathcal{F}(0)e^{-t/\tau_i}\right.$$
$$\left. + \int_0^t \mathcal{F}'(\xi)e^{-(t-\xi)/\tau_i}\,d\xi\right], \qquad (7)$$

where τ_i, a_i, and ϕ_i are parameters depending on C, C_0, γ, and λ. Their expressions are given in Table 1. Note, in particular, that $a_f + a_s = 1$ and $\phi_f a_f + \phi_s a_s = 1$, and that $\phi_f < 0$ while a_f, a_s, and ϕ_s are all positive.

The sum term in Eq. (6) is the heat-uptake temperature T_H. It is the sum of two modes that can be decomposed in two terms depending on the forcing function. The first contribution is an instantaneous deviation associated with a discontinuity of the forcing at $t = 0$. The second term is due to the time evolution of the forcing.

In the following paragraphs, we briefly discuss the analytical solution for two idealized forcings, step and linear. In appendixes C and D, we present solutions for stabilization, abrupt return to zero, and periodic forcings.

1) STEP FORCING

For a step forcing,

$$\mathcal{F}(t) = \begin{cases} 0 & \text{if} \quad t < 0 \\ \mathcal{F} & \text{if} \quad t \geq 0 \end{cases}, \qquad (8)$$

the analytical solution of the two-layer energy-balance model is given by

TABLE 1. Summary of definitions of two-layer model general and mode parameters and relationships between mode and physical parameters.

Definition of general parameters
$b = \dfrac{\lambda + \gamma}{C} + \dfrac{\gamma}{C_0}$
$b^* = \dfrac{\lambda + \gamma}{C} - \dfrac{\gamma}{C_0}$
$\delta = b^2 - 4\dfrac{\lambda\gamma}{CC_0}$

Mode parameters	
Fast	Slow
$a_f = \dfrac{\phi_s \tau_f}{C(\phi_s - \phi_f)}\lambda$	$a_s = -\dfrac{\phi_f \tau_s}{C(\phi_s - \phi_f)}\lambda$
$\phi_f = \dfrac{C}{2\gamma}(b^* - \sqrt{\delta})$	$\phi_s = \dfrac{C}{2\gamma}(b^* + \sqrt{\delta})$
$\tau_f = \dfrac{CC_0}{2\lambda\gamma}(b - \sqrt{\delta})$	$\tau_s = \dfrac{CC_0}{2\lambda\gamma}(b + \sqrt{\delta})$
$l_f = a_f \tau_f \dfrac{\lambda}{C + C_0}$	$l_s = a_s \tau_s \dfrac{\lambda}{C + C_0}$

Relationships between parameters
$a_f + a_s = 1$
$a_f/\tau_f + a_s/\tau_s = \lambda/C$
$\tau_f a_f + \tau_s a_s = (C + C_0)/\lambda$
$\tau_f a_s + \tau_s a_f = C_0/\gamma$
$\phi_f a_f/\tau_f + \phi_s a_s/\tau_s = 0$
$\tau_f \tau_s = CC_0/(\lambda\gamma)$
$C + \phi_f C_0 = \lambda\tau_f$
$C + \phi_s C_0 = \lambda\tau_s$
$\phi_f a_f + \phi_s a_s = 1$
$\phi_f \phi_s = -C/C_0$

$$T(t) = \frac{\mathcal{F}}{\lambda}[a_f(1 - e^{-t/\tau_f}) + a_s(1 - e^{-t/\tau_s})] \quad \text{and} \quad (9)$$

$$T_0(t) = \frac{\mathcal{F}}{\lambda}[\phi_f a_f(1 - e^{-t/\tau_f}) + \phi_s a_s(1 - e^{-t/\tau_s})]. \quad (10)$$

By decomposing the response as the sum of the equilibrium temperature response and the two modes characterized by the two distinct time scales, τ_f (fast) and τ_s (slow) following Eqs. (6) and (7), the temperature perturbations T and T_0 are

$$T(t) = T_{eq} - a_f T_{eq} e^{-t/\tau_f} - a_s T_{eq} e^{-t/\tau_s} \quad \text{and} \quad (11)$$

$$T_0(t) = T_{eq} - \phi_f a_f T_{eq} e^{-t/\tau_f} - \phi_s a_s T_{eq} e^{-t/\tau_s}. \quad (12)$$

The sums of the last two terms of Eqs. (11) and (12) are respectively the perturbations $T_H(t) = T(t) - T_{eq}$ and $T_{0H}(t) = T_0(t) - T_{eq}$ from the new equilibrium $T = T_0 = T_{eq}$. Thus, a_i is the partial contribution of the mode i to the T_H initial amplitude in the case of a step forcing. Initially, both the slow and the fast terms of T_H are negative with respective amplitudes $-a_f T_{eq}$ and $-a_s T_{eq}$.

During the transition, they increase exponentially toward zero with their respective relaxation times τ_f and τ_s as illustrated in Figs. 1a and 1b.

Since $\phi_s > 0$, the slow contributions of T_H and T_{0H} have the same sign, and the slow mode corresponds to a joint adjustment of the upper and lower layers. On the other hand, since $\phi_f < 0$, the fast mode of T_{0H} is of opposite sign to the slow mode of T_H (in the fast mode, $T_H < 0$ and $T_{0H} > 0$). The perturbation heat flux from the lower layer to the upper layer is $-H = -\gamma(T_H - T_{0H})$ and its fast mode is of opposite sign to T_H. The fast mode thus corresponds to an adjustment of the upper layer by both the radiation imbalance and the deep-ocean heat uptake. The two physical processes at play interact positively to adjust the smallest energy reservoir. This explains why the characteristic time scale τ_f is shorter than the characteristic time scale of a one-layer model of the upper layer without deep-ocean heat uptake (i.e., the limit of τ_f when C_0 tends toward zero; $\tau_f < C/\lambda$). Still, τ_f is longer than the characteristic time scale of the one-layer model with the deep-ocean heat-uptake formulation of Gregory and Mitchell (1997) and Raper et al. (2002) that is the limit of τ_f when C_0 tends toward infinity $\tau_f > C/(\gamma + \lambda)$. In that model, the deep-ocean heat uptake damps T_H more efficiently than in the two-layer model because of its infinite heat capacity. For a system with a vanishingly small upper-ocean heat capacity, the adjustment of the first layer is immediate leading to a slightly faster adjustment of the deep ocean. Indeed, the slow time scale is longer than its limit when C tends toward zero $\tau_s > C_0(1/\lambda + 1/\gamma)$.

2) LINEAR FORCING

To derive the analytical solution of the system for a linear forcing

$$\mathcal{F}(t) = \begin{cases} 0 & \text{if } t < 0 \\ kt & \text{if } t \geq 0 \end{cases}, \quad (13)$$

Eqs. (6) and (7) require the knowledge of the integral $\mathcal{I}(t) = \int_0^t \xi e^{\xi/\tau_i} d\xi$, which is $\mathcal{I}(t) = \tau_i t e^{t/\tau_i} + \tau_i^2(1 - e^{t/\tau_i})$. Then the general solution can be written as

$$T(t) = \frac{k}{\lambda}t - \frac{k}{\lambda}\tau_f a_f(1 - e^{-t/\tau_f}) - \frac{k}{\lambda}\tau_s a_s(1 - e^{-t/\tau_s}) \quad \text{and}$$
$$(14)$$

$$T_0(t) = \frac{k}{\lambda}t - \frac{k}{\lambda}\phi_f \tau_f a_f(1 - e^{-t/\tau_f}) - \frac{k}{\lambda}\phi_s \tau_s a_s(1 - e^{-t/\tau_s}).$$
$$(15)$$

As in the step-forcing case, the surface temperature perturbation is the sum of an instantaneous equilibrium temperature response $T_{eq}(t) = \mathcal{F}(t)/\lambda$ and an imbalance
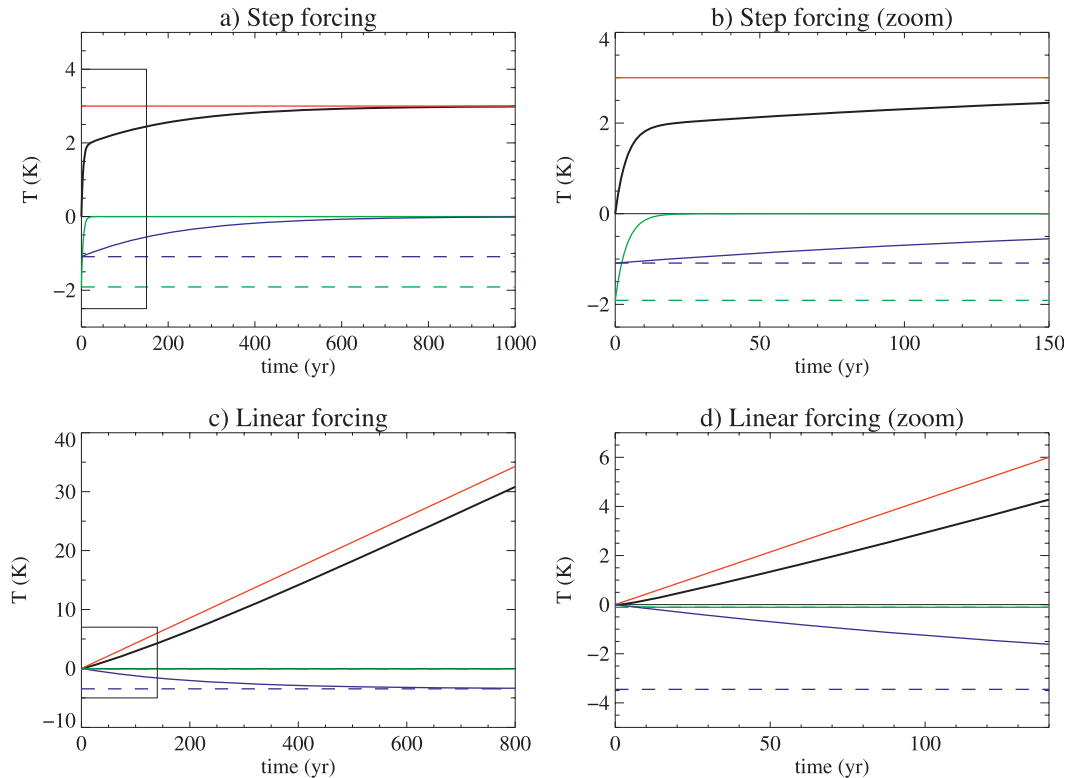
FIG. 1. Mean surface temperature response (thick solid black line) and its decomposition in three components [see Eqs. (11) and (14)], the equilibrium component (solid red line), the fast (solid green line), and the slow (solid blue line) modes, as a function of time for (a),(b) a step forcing and (c),(d) a linear forcing. The dashed green and blue lines denote the fast and slow modes' amplitude, respectively. In (b) and (d), we zoom in on the black boxes indicated in (a) and (c), respectively. Values are for $\mathcal{F} = 3.9$ W m^{-2}, $\lambda = 1.3$ W m^{-2} K^{-1}, $C = 8$ W yr m^{-2} K^{-1}, $C_0 = 100$ W yr m^{-2} K^{-1}, and $\gamma = 0.7$ W m^{-2} K^{-1}.

term that can be decomposed into a fast and a slow mode response as illustrated in Figs. 1c and 1d. Contrary to the abrupt case, the system is initially in equilibrium and deviates from its instantaneous equilibrium afterward. The fast and slow responses decrease with time and asymptotically tend toward negative limits. Their amplitudes are proportional to their respective relaxation times, resulting in a small amplitude of the fast response.

Assuming a logarithmic relationship between the radiative forcing and the carbon dioxide concentration [Eq. (3)], the 1% yr^{-1} CO$_2$ experiment corresponds to a linear forcing

$$k = \frac{\mathcal{F}_{2\times CO_2}}{t_{2\times CO_2}} \quad \text{with} \quad t_{2\times CO_2} \approx 70 \, \text{yr}. \quad (16)$$

3. Multimodel analysis

In this section, a method to tune the two-layer model parameters described above to fit the behavior of each AOGCM using only the idealized step-forcing

experiments is proposed. The calibration method is then applied to 16 available AOGCMs participating in the CMIP5 (Taylor et al. 2011) and is validated by using the AOGCM responses to the linear forcing 1% yr^{-1} CO$_2$ experiments.

a. Method for parameter calibration

The method uses only the transient response of an AOGCM step-forcing experiment. We assume that the top of the climate system corresponds to the model top of the atmosphere (TOA). Both radiative net flux change at TOA and surface temperature change T are used to adjust the two radiative parameters $\mathcal{F}_{\text{ref}}$ (the adjusted radiative forcing amplitude) and λ. Only T is used to adjust the thermal inertia parameters C, C_0, and γ. The method can thus be decomposed in two steps.

1) FIRST STEP

The first step consists of estimating the radiative parameters $\mathcal{F}_{\text{ref}}$ and λ by performing a linear regression of the radiative imbalance as a function of the mean

TABLE 2. Complete model expansions.

Model	Expansion
BCC-CSM1–1	Beijing Climate Center, Climate System Model, 1-1
BNU-ESM	Beijing Normal University - Earth System Model
CanESM2	Canadian Earth System Model, version 2
CCSM4	Community Climate System Model, version 4
CNRM-CM5	Centre National de Recherches Météorologiques Coupled Global Climate Model, version 5
CSIRO-Mk3.6.0	Commonwealth Scientific and Industrial Research Organisation Mark, version 3.6.0
FGOALS-s2	Flexible Global Ocean-Atmosphere-Land System Model gridpoint, second spectral version
GFDL-ESM2M	Geophysical Fluid Dynamics Laboratory Earth Science Model 2M
GISS-E2-R	Goddard Institute for Space Studies Model E, coupled with Russell ocean model
HadGEM2-ES	Hadley Centre Global Environmental Model 2, Earth System
INM-CM4	Institute of Numerical Mathematics Coupled Model, version 4.0
IPSL-CM5A-LR	L'Institut Pierre-Simon Laplace Coupled Model, version 5, coupled with NEMO, low resolution
MIROC5	Model for Interdisciplinary Research on Climate, version 5
MPI-ESM-LR	Max Planck Institute Earth System Model, low resolution
MRI-CGCM3	Meteorological Research Institute Coupled General Circulation Model, version 3
NorESM1-M	Norwegian Earth System Model, intermediate resolution

surface air temperature perturbation (Gregory et al. 2004). Using this method, the computation of $\mathcal{F}_{ref}$ and λ takes into account both stratospheric and tropospheric adjustments. However it assumes a linear dependence between the earth's radiative imbalance and the surface temperature perturbation such that $N = \mathcal{F} - \lambda T$. The limitations of this assumption are discussed in Part II.

2) SECOND STEP

The second step consists first of the calibration of the four mode parameters τ_f, τ_s, a_f, and a_s by fitting the global mean surface air temperature response. For $t \gg \tau_f$, Eq. (11) can be approximated as follows:

$$T \approx T_{eq}(1 - a_s e^{-t/\tau_s}) \Rightarrow \log\left(1 - \frac{T}{T_{eq}}\right) \approx \log a_s - \frac{1}{\tau_s}t. \tag{17}$$

Assuming that $\tau_f \ll 30$ yr, the linear regression of $\log(T_{eq} - T)$ against t over the period 30–150 yr gives estimates of τ_s and a_s.

Then $a_f = 1 - a_s$ is known and τ_f can be expressed from Eq. (11) as a function of these three parameters and the surface temperature response

$$\tau_f = t/[\log a_f - \log(1 - T/T_{eq} - a_s e^{-t/\tau_s})]. \tag{18}$$

Its value is estimated by averaging over the first 10 years of the step-forcing experiment.

Finally, the remaining physical parameters of the model (the heat capacities C and C_0 and the heat exchange coefficient γ) are computed from the other parameters using the following analytical relationships (see Table 1):

$$C = \lambda/(a_f/\tau_f + a_s/\tau_s), \tag{19}$$

$$C_0 = \lambda(\tau_f a_f + \tau_s a_s) - C, \quad \text{and} \tag{20}$$

$$\gamma = C_0/(\tau_f a_s + \tau_s a_f). \tag{21}$$

This methodology is applied to instantaneous carbon dioxide quadrupling (abrupt $4\times CO_2$) experiments (with a typical integration time of 150 yr) performed by an ensemble of 16 AOGCMs participating in CMIP5. Note that we use annual mean values over a period of 150 years even when longer simulations are provided. The name of the AOGCMs used and their expansions are provided in Table 2.

b. Results

1) RADIATIVE PARAMETERS

For the 16 AOGCMs considered here, the radiative parameters and the $4\times CO_2$ equilibrium temperature response are reported in Table 3. The results are in good agreement with the estimates of Andrews et al. (2012). The multimodel average of the net radiative forcing (6.9 W m^{-2}) is very close to previous CMIP3 analysis results (Williams et al. 2008), and the relative intermodel standard deviation is about 13%. The estimates for the model's feedback parameters are consistent with previous results with older AOGCMs (Soden and Held 2006). The multimodel mean (1.13 W m^{-2} K^{-1}) and standard deviation (0.31 W m^{-2} K^{-1}) of the total feedback parameters (Table 3) are close to previous values obtained for CMIP3 models and for different types of scenarios. The $4\times CO_2$ equilibrium temperature response ranges from 4.1 to 9.1 K. The spread among the responses is as large as those of CMIP3 simulations.

TABLE 3. The $4\times CO_2$ radiative forcing $\mathcal{F}_{4\times CO_2}$, radiative feedback parameter λ for a CO_2 perturbation, and $4\times CO_2$ equilibrium temperature $T_{4\times CO_2}$ estimates of the 16 CMIP5 models studied in this paper, and their multimodel mean and standard deviation. The version of the model used in this study is also indicated (complete model expansions are provided in Table 2).

Model	$\mathcal{F}_{4\times CO_2}$ (W m^{-2})	λ (W m^{-2} K^{-1})	$T_{4\times CO_2}$ (K)
BCC-CSM1–1	6.7	1.21	5.6
BNU-ESM	7.4	0.93	8.0
CanESM2	7.6	1.03	7.4
CCSM4	7.2	1.24	5.8
CNRM-CM5	7.3	1.11	6.5
CSIRO-Mk3.6.0	5.1	0.61	8.3
FGOALS-s2	7.5	0.88	8.5
GFDL-ESM2M	6.6	1.34	4.9
GISS-E2-R	7.3	1.70	4.3
HadGEM2-ES	5.9	0.65	9.1
INM-CM4	6.2	1.51	4.1
IPSL-CM5A-LR	6.4	0.79	8.1
MIROC5	8.5	1.58	5.4
MPI-ESM-LR	8.2	1.14	7.3
MRI-CGCM3	6.6	1.26	5.2
NorESM1-M	6.2	1.11	5.6
Multimodel mean	6.9	1.13	6.5
Standard deviation	0.9	0.31	1.6

2) CLIMATE SYSTEM INERTIA PARAMETERS

In Table 4, we summarize the corresponding thermal parameters for each of the 16 models. We first note that the deep-ocean heat-capacity values are about an order of magnitude larger than the upper-layer heat-capacity values. The multimodel means of C (7.3 W yr m^{-2} K^{-1}) and C_0 (106 W yr m^{-2} K^{-1}) are close to the estimates of Dickinson (1981) of 10 and 100 W yr m^{-2} K^{-1} for the ocean mixed layer and for the deep-ocean capacities respectively. The deep-ocean heat-capacity mean value is, however, larger than the estimate of Murphy (1995) for the ocean capacity of about 52 W yr m^{-2} K^{-1} (1.65 10^9 J m^{-2} K^{-1}). Considering that the ocean covers $f_0 = 70\%$ of the Earth's surface, and using a constant water heat capacity of $c_p = 4180$ J kg^{-1} K^{-1} and a constant density of saltwater $\rho = 1030$ kg m^{-3}, the AOGCM ensemble mean C_0 value corresponds to an equivalent deep-ocean layer depth D_0 equal to

$$D_0 = \frac{86\,400 \times 365.25 \times C_0}{\rho c_p f_0} = 1105 \text{ m}. \quad (22)$$

Similarly, an upper ocean with an effective heat capacity equal to the AOGCM ensemble mean value is equivalent to a 77-m-thick mixed layer.

The INM-CM4 model gives a very large value of C_0 (317 W yr m^{-2} K^{-1}) in comparison with other models. One can wonder if this estimation can be biased by the drift in surface temperature evolution since the INM-CM4 model is one of the two models with the largest drift in surface temperature evolution in the course of the preindustrial control simulation. Indeed, the INM-CM4 drift is on the order of -0.03 K century^{-1} (over a

TABLE 4. The atmosphere/land/upper-ocean heat capacity C, deep-ocean heat capacity C_0, heat exchange coefficient γ, and fast and slow relaxation times estimates of the 16 CMIP5 models used in this paper, and their multimodel mean and standard deviation given for the 16 models ensemble and by excluding the INM-CM4 model.

Model	C (W yr m^{-2} K^{-1})	C_0 (W yr m^{-2} K^{-1})	γ (W m^{-2} K^{-1})	τ_f (yr)	τ_s (yr)
BCC-CSM1–1	7.6	53	0.67	4.0	126
BNU-ESM	7.4	90	0.53	5.0	267
CanESM2	7.3	71	0.59	4.5	193
CCSM4	6.1	69	0.93	2.8	132
CNRM-CM5	8.4	99	0.50	5.2	289
CSIRO-Mk3.6.0	6.0	69	0.88	3.9	200
FGOALS-s2	7.0	127	0.76	4.2	317
GFDL-ESM2M	8.1	105	0.90	3.6	197
GISS-E2-R	4.7	126	1.16	1.6	184
HadGEM2-ES	6.5	82	0.55	5.3	280
INM-CM4	8.6	317	0.65	4.0	698
IPSL-CM5A-LR	7.7	95	0.59	5.5	286
MIROC5	8.3	145	0.76	3.5	285
MPI-ESM-LR	7.3	71	0.72	3.9	164
MRI-CGCM3	8.5	64	0.66	4.3	150
NorESM1-M	8.0	105	0.88	4.0	218
Multimodel mean	7.3	106	0.73	4.1	249
- without INM-CM4	7.3	91	0.74	4.1	219
Standard deviation	1.1	62	0.18	1.0	135
- without INM-CM4	1.1	27	0.18	1.0	63

period of 500 yr) against a model ensemble mean absolute value of 0.02 K century^{-1} and a standard deviation of 0.014 K century^{-1}. However, after removing the temperature trend, the C_0 estimate for INM-CM4 still remains largely outside the range of the model ensemble with a value of 271 W yr m^{-2} K^{-1}. All other parameters of this model and all the parameters of the other models are not significantly impacted by the temperature drift correction. Further investigation would be needed to explain the INM-CM4 behavior. By excluding this model, the ensemble mean C_0 value is 91 W yr m^{-2} K^{-1} with a much smaller standard deviation of 27 W yr m^{-2} K^{-1}.

The heat exchange coefficient γ ranges from 0.5 to 1.2 W m^{-2} K^{-1} (0.9 W m^{-2} K^{-1} without the GISS-E2-R model) with an ensemble mean of about 0.7 W m^{-2} K^{-1}. These values are somewhat larger than the zero-layer EBM heat exchange coefficient κ values estimated by Raper et al. (2002) and Gregory and Forster (2008) and of the same order of magnitude as the estimates of Plattner et al. (2008). One could expect that the introduction of the deep-ocean temperature perturbation T_0 in the two-layer EBM reduces the contribution of the temperature difference term to the deep-ocean heat uptake $H = \gamma(T - T_0)$ formulation (for a given H: $T - T_0 < T$, so that $\gamma > \kappa$).

Fast and slow time responses are also given in Table 4. The fast time constant is on the order of 4 yr and the slow response is on the order of 250 yr. These values are consistent with previous estimations of climate system time scales (see, e.g., Olivié et al. 2012). The intermodel standard deviation for the slow relaxation time is about 135 yr. It is reduced to 63 yr by omitting the large value of τ_s (caused by the large C_0) of the INM-CM4 model.

The estimates of these climate system parameters could be biased as a consequence of the biases in the radiative parameters estimated using the method of Gregory et al. (2004). The sensitivity of these estimates to a more refined formulation of the two-layer model is explored in Part II.

3) GLOBAL MEAN SURFACE AIR TEMPERATURE RESPONSE

The comparison between the analytical model calibrated from abrupt 4×CO$_2$, the AOGCM responses to the abrupt 4×CO$_2$, and the AOGCM responses to the 1% yr^{-1} CO$_2$ increase up to 4×CO$_2$ is shown in Fig. 2. For CNRM-CM5 and GFDL-ESM2M, a 2×CO$_2$ stabilization scenario is also available. Note that the analytical EBM results for the 1% yr^{-1} CO$_2$ and the stabilization cases are computed using the parameters tuned using the abrupt 4×CO$_2$ experiment, and are therefore independent of the corresponding AOGCM experiments. All

values are temperature change with respect to the mean control values over the whole 150-yr period.

The simple analytical model is able to reproduce the evolution of surface air temperature in response to both a step-forcing and a gradual-forcing scenario. The fit seems to accurately represent the behavior of the surface temperature in a case of an abrupt forcing, not only at the beginning and at the end of the period (used in the tuning), but also in the intermediate period of transition between the two modes. However, for some models, a slight overestimation is observed for the 1% yr^{-1} CO$_2$ scenario (CSIRO-Mk3.6.0, MIROC5, MPI-ESM-LR, NorESM1-M) and for the 2×CO$_2$ stabilization (GFDL-ESM2M). It may be due to the imperfect logarithmic dependency between the radiative forcing and the carbon dioxide concentration (e.g., because of tropospheric adjustment) or to limitations inherent to the linear two-layer model such as the use of a single feedback parameter for all radiative forcing amplitudes, the assumption of linearity between the radiative imbalance, and the surface temperature change during a climate transition, or an oversimplified representation of ocean heat uptake.

It is possible that using a median scenario to fit the EBM's parameters would give more accurate results. The abrupt 4×CO$_2$ case is an extreme case and an intermediate CO$_2$ increase scenario such as a doubling of carbon dioxide concentration may give more adequate results. Overall, it appears that the climate response depicted by the AOGCMs can be captured by a properly tuned two-layer climate model.

c. Upper- and deep-ocean heat-uptake contributions to the fast and slow responses

In this section, the concepts of upper- and deep-ocean heat-uptake temperatures are introduced. The heat-uptake temperature T_H [Eq. (5)] can be decomposed into the sum of an upper-ocean heat-uptake temperature T_U and a deep-ocean heat-uptake temperature T_D with

$$T_U = -\frac{1}{\lambda}C\frac{dT}{dt} \quad \text{and} \tag{23}$$

$$T_D = -\frac{1}{\lambda}C_0\frac{dT_0}{dt}. \tag{24}$$

The contribution of these two components to the fast and the slow responses are quantitatively examined for two forcing functions.

1) STEP FORCING

In the case of a step forcing, by using Eq. (5), the heat-uptake temperature T_H is

$$T_H(t) = -\frac{1}{\lambda}C\frac{dT}{dt} - \frac{1}{\lambda}C_0\frac{dT_0}{dt}$$
$$= -\frac{\mathcal{F}}{\lambda^2}\left(\frac{C+\phi_f C_0}{\tau_f}a_f e^{-t/\tau_f} + \frac{C+\phi_s C_0}{\tau_s}a_s e^{-t/\tau_s}\right). \tag{25}$$

The heat-uptake temperature tends exponentially to zero with slow and fast relaxation times

$$T_H(t) = -\frac{\mathcal{F}}{\lambda}[(f_U+f_D)a_f e^{-t/\tau_f} + (s_U+s_D)a_s e^{-t/\tau_s}], \tag{26}$$

with $f_U + f_D = 1$ and $s_U + s_D = 1$. Each mode (slow and fast) is respectively written as the sum of the contribution of each component heat uptake (the subscript U refers to the first layer and the subscript D to the second layer). Indeed, f_U (f_D) and s_U (s_D) are the partial contributions of the upper (deep) component respectively to the fast and the slow responses in:

$$T_U(t) = -\frac{\mathcal{F}}{\lambda}(f_U a_f e^{-t/\tau_f} + s_U a_s e^{-t/\tau_s}) \quad \text{and} \tag{27}$$

$$T_D(t) = -\frac{\mathcal{F}}{\lambda}(f_D a_f e^{-t/\tau_f} + s_D a_s e^{-t/\tau_s}), \tag{28}$$

where

$$f_U = \frac{C}{\lambda\tau_f}, \quad f_D = \frac{\phi_f C_0}{\lambda\tau_f}, \quad s_U = \frac{C}{\lambda\tau_s}, \quad \text{and} \quad s_D = \frac{\phi_s C_0}{\lambda\tau_s}. \tag{29}$$

The order of magnitude and the sign of the fractional contributions are given in section 3c(3).

2) LINEAR FORCING

In the case of a linear forcing, the heat-uptake temperature is

$$T_H(t) = -\frac{k}{\lambda^2}\left[C+C_0 - \sum_{i=\{s,f\}}(C+\phi_i C_0)a_i e^{-t/\tau_i}\right], \tag{30}$$

which can be rewritten as

$$T_H(t) = -\frac{k}{\lambda}\frac{C+C_0}{\lambda}[h_U + h_D - (f_U+f_D)l_f e^{-t/\tau_f} - (s_U+s_D)l_s e^{-t/\tau_s}], \tag{31}$$

where l_f and l_s are a fractional contribution of the fast and the slow terms ($l_f + l_s = 1$). Their expression is given in Table 1. Note that f_U, f_D, s_U, and s_D are the same as previously, and $h_U = C(C + C_0)$ and $h_D = C_0(C + C_0)$ correspond to the fractional contribution of upper and lower layers to the asymptotic heat-uptake temperature, which is proportional to the sum of the two heat capacities

$$T_H(t) \rightarrow \hat{T}_H = -\frac{k}{\lambda}\frac{C+C_0}{\lambda}(h_U + h_D) = -\frac{k}{\lambda}\frac{C+C_0}{\lambda}. \tag{32}$$

3) QUANTITATIVE ESTIMATES OF FRACTIONAL CONTRIBUTIONS

Figure 3a shows the fractional contributions of the fast and slow modes to the maximum amplitude of the heat-uptake temperature for the step forcing, a_f and a_s. For all models except one (CSIRO-Mk3.6.0), the percentage of T_H caused by the fast response is larger than that caused by the slow response for a step forcing but with a similar order of magnitude. The multimodel mean value of a_f is 59%.

The contributions of the upper- and lower-layer heat uptake to the fast (f_U and f_D) and the slow (s_U and s_D) terms are depicted in Figs. 3b and 3c. For the fast mode, the role of the two components of the system is opposite but with similar amplitude. For all models, the amplitude of the atmosphere/land/upper-ocean contribution T_U is larger than that of the deep ocean. For the slow mode, the contribution of T_U is negligible (i.e., $s_U \ll s_D$). Then, the temperature slow response is driven exclusively by the deep-ocean heat uptake.

The fast and slow modes of the deep-ocean heat-uptake temperature T_D are of opposite sign with equal initial amplitude. During a step-forcing transient regime, T_D decreases from zero toward negative values (the heat uptake H increases from zero) until the fast mode becomes negligible. Then T_D increases slowly and tends asymptotically toward zero. This nonmonotonic time evolution results from the fact that the surface and the deep-ocean temperature perturbations T and T_0 associated to the fast response have opposite signs ($\phi_f < 0$). The heat flux between the lower and upper layer is upward: the deep ocean warms the surface in the fast response, as pointed out in section 2b(1).

In the case of a linear forcing, the contribution l_f of the fast term is negligible (Fig. 3d) with a multimodel mean value of 0.03%, because the fractional amplitudes l_f and l_s are proportional to their respective relaxation times. The heat-uptake temperature is driven by the deep-ocean heat-uptake temperature slow term ($s_U \ll s_D$) and by the asymptotic term $\hat{T}_H$. The upper-ocean heat-uptake
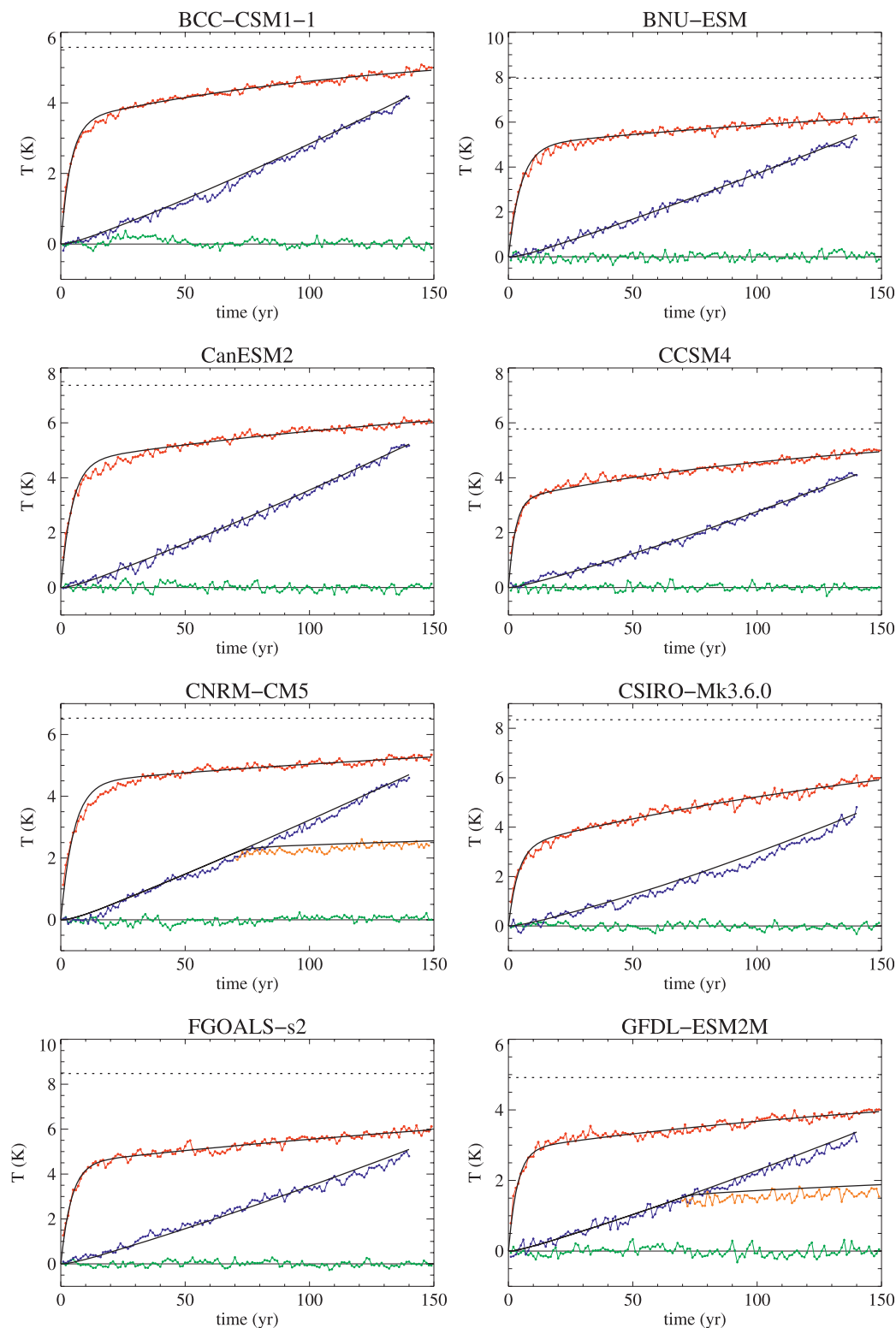
FIG. 2. Time series of global mean and annual mean surface air temperature change of the abrupt $4\times CO_2$ (red line), the 1% yr^{-1} CO_2 (until $4\times CO_2$) (blue line), the $2\times CO_2$ stabilization (when available; orange line), and the control (green line) CMIP5 experiments for the 16 AOGCMs and of the corresponding EBM analytical temperature change evolutions (black lines) calibrated only with the abrupt $4\times CO_2$ experiment. For each model, the black dotted line indicates the estimated equilibrium temperature response $T_{4\times CO_2}$ of a $4\times CO_2$ perturbation. All values are temperature changes with respect to the mean control value over the whole 150-yr period. Note that the scale of the y axis can differ from one panel to another.

GISS−E2−R

HadGEM2−ES

INMCM4

IPSL−CM5A−LR

MIROC5

MPI−ESM−LR

MRI−CGCM3

NorESM1−M
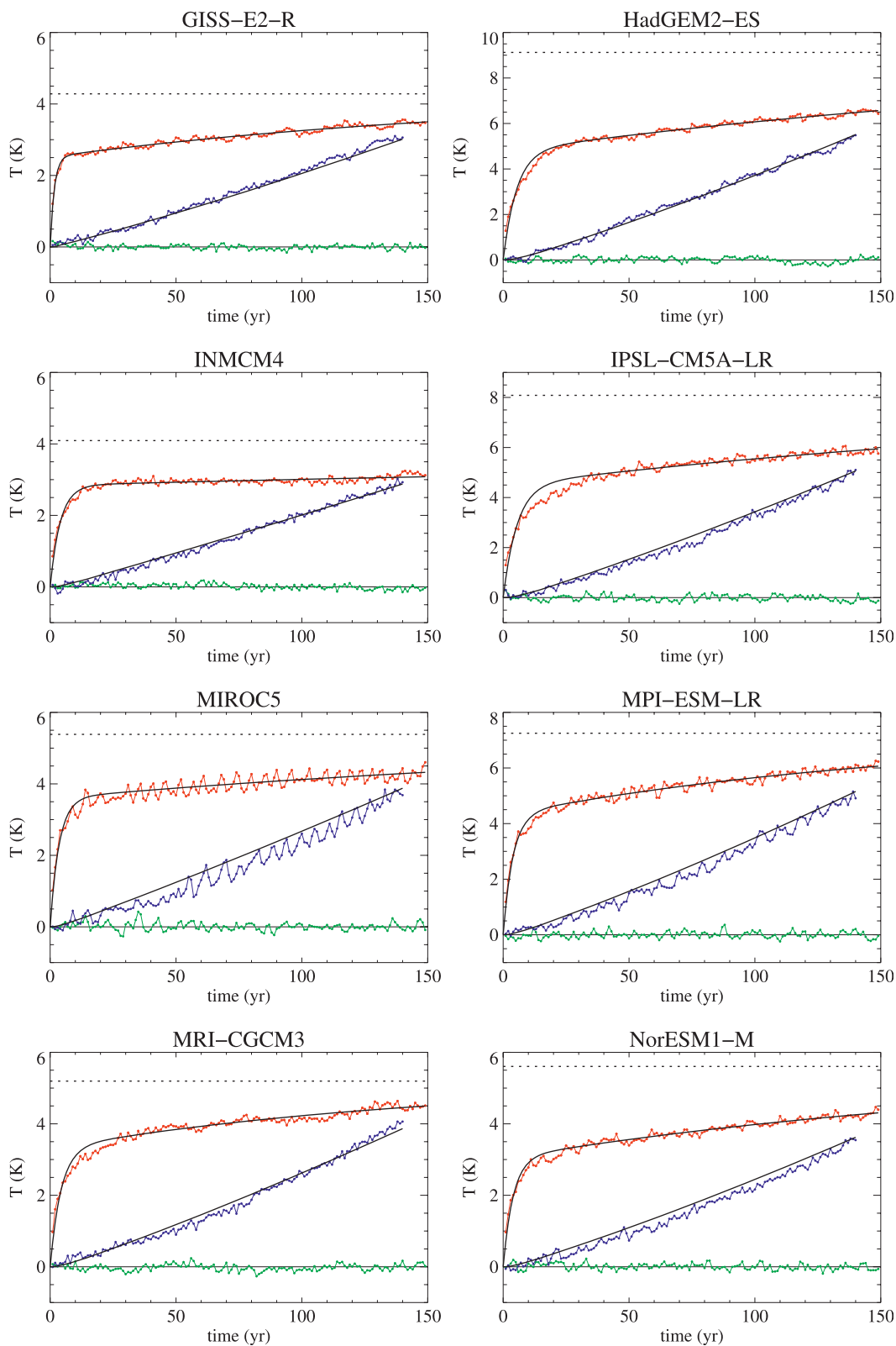
FIG. 2. (*Continued*)
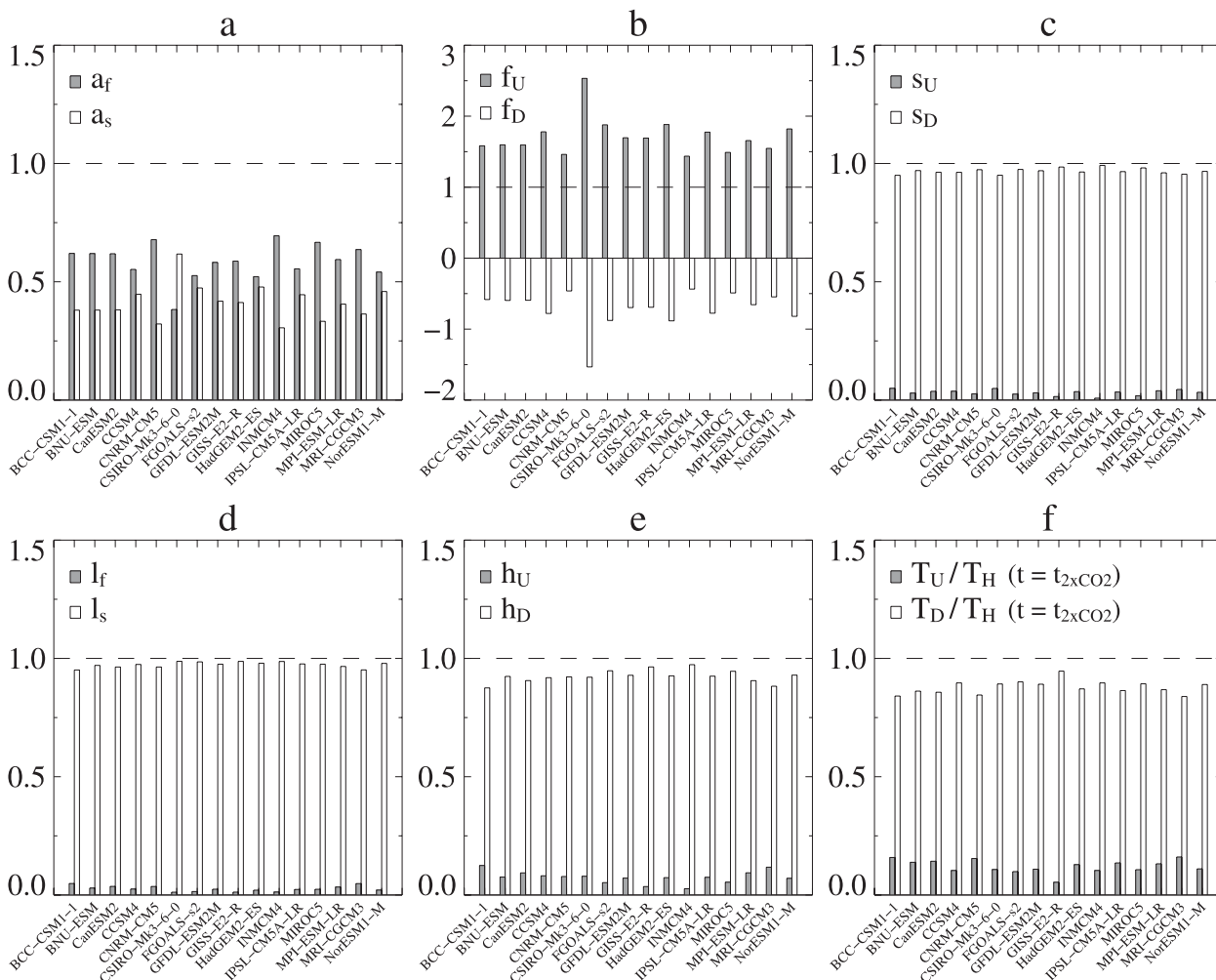
FIG. 3. Multimodel values of (a) the mode parameters (a_f, a_s), the upper-ocean and deep-ocean heat-uptake temperatures' contribution to (b) the fast mode (f_U, f_D) and (c) the slow mode (s_U, s_D), (d) the mode parameters (l_f, l_s) in response to a linearly increasing forcing, (e) the upper-ocean and deep-ocean heat-uptake temperatures' contribution to the linear-forcing asymptotic term (h_U, h_D), and (f) the ratios T_U/T_H and T_D/T_H at the time of $2\times CO_2$ for the 1% yr^{-1} CO_2 experiment.

temperature fast term reaches its asymptotic value, which represents on average 8% of the asymptotic heat-uptake temperature $\hat{T}_H$. Figure 3e shows the multimodel contributions to $\hat{T}_H$ of both upper ocean and deep ocean. However, on a centennial scale, the asymptotic deep-ocean heat-uptake temperature is not reached. As a result, the contribution of T_D relative to T_U is smaller during the transient regime (Fig. 3f). The upper-ocean heat-uptake temperature T_U is on average 18% of the heat-uptake temperature at the time of $2\times CO_2$ ($t = 70$ yr) and 12% at the time of $4\times CO_2$ ($t = 140$ yr). Removing the upper-ocean heat-uptake contribution, the transient climate response (i.e., T at the time of $2\times CO_2$) would be on average 11% larger, which corresponds to a temperature difference on average of 0.2 K (and a range of 0.1–0.4 K).

4. Conclusions

In this study, we describe the analytical solutions of a two-layer energy-balance model for different idealized forcings and propose a method to tune the parameters of this simple climate model to reproduce the behavior of individual coupled atmosphere–ocean general circulation models. In this simple idealized framework, the global mean surface response change consists of the sum of an instantaneous equilibrium temperature and a disequilibrium temperature, the heat-uptake temperature, which is a sum of two modes. One mode responds very quickly to changes in forcing, whereas the other mode has a longer relaxation time.

By analyzing the results of 16 AOGCM's experiments from CMIP5, we show that this decomposition

in an equilibrium term and two modes can be derived for any AOGCM by a calibration method using only a step-forcing scenario. We first show that this decomposition can reproduce well the behavior of AOGCM's response to a step $4\times CO_2$ forcing scenario over the 150-yr period covered by the CMIP5 simulations. We also find that the simple model calibrated with a step-forcing experiment is able to represent gradual CO_2-increase idealized scenarios because the analytic response exhibits a satisfactory fit for the scenario with a 1% yr^{-1} CO_2 increase and stabilization when available. We found the clear separation of time scales highlighted by Held et al. (2010), since the fast relaxation time multimodel mean is about 4 yr while the slow time scale is about 250 yr.

An analysis of the contribution of the two layers' heat uptake to the fast and the slow modes shows that the upper-ocean heat uptake contributes only to the fast mode that is shown to be quite small in the case of a linear forcing. In the case of a step forcing, both layers' heat uptakes contribute to the response amplitude and the upper-ocean heat uptake plays a key role in the representation of the first stages of the temperature and radiative flux responses. Thus, this contribution is important to estimate the amplitude of the forcing from a step-forcing experiment. Moreover, an accurate representation of the temperature response near equilibrium is necessary to estimate the equilibrium climate sensitivity. The two-layer EBM is the simplest tool that incorporates both of these features, and is therefore the simplest adequate model to simulate transient climate change under all kinds of idealized scenarios.

However, a main limitation of the simple model used in this study is the intrinsic assumption of a linear dependence between the radiation imbalance at the TOA and the mean surface temperature perturbation. In Part II, the two-layer EBM with an efficacy factor of deep-ocean heat uptake proposed in Held et al. (2010) is used to overcome this problem and applied to CMIP5 AOGCMs.

APPENDIX A

Analogy with Electricity

The two-layer energy-balance model and its simpler (one-layer model) version can be advantageously described in terms of equivalent electrical circuits (Fig. A1). While temperature differences are analogous to electrical potential differences, heat fluxes are analogous to currents.

In the case of the one-layer model (see Fig. A1a), the first layer is a capacitor with capacity C. It is linked to the external system by a resistance $1/\lambda$ and to the second layer by a resistance $1/\kappa$. The output voltage (the voltage across the capacitor) is the mean surface air temperature T. The input voltage is equal to the instantaneous equilibrium temperature $T_{eq}(t) = \mathcal{F}(t)/\lambda$. The current in the main branch of the circuit (the left-hand branch) is the radiative imbalance $N = \mathcal{F} - \lambda T$. For a step forcing, the capacitor voltage increases until saturation. The current through the capacitor becomes zero and the equilibrium temperature response is given by a voltage divider and is equal to $\mathcal{F}/(\lambda + \kappa)$.

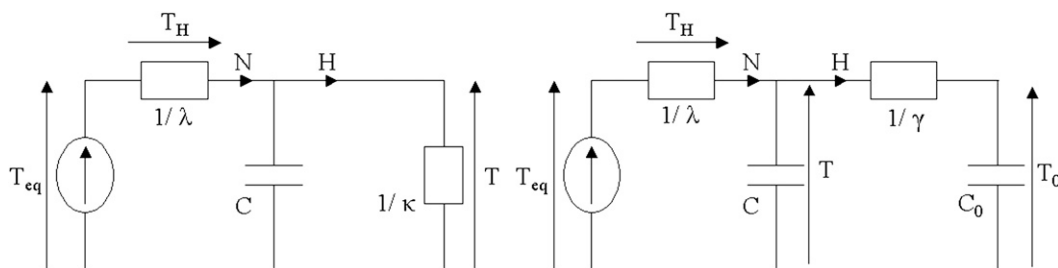In the case of the two-layer model (see Fig. A1b), there is a resistance $1/\gamma$ and an additional capacitor

FIG. A1. Analogous electrical circuit of the (left) one-layer and (right) two-layer energy-balance models.

with a higher capacity value C_0 in the secondary branch through which the current analogous to the deep-ocean heat uptake flows. The deep-ocean temperature perturbation T_0 is the voltage across this capacitor. In equilibrium, both currents are zero and $T = T_0 = T_{eq}$.

Both circuits are low-pass filters. The Bode diagram of the second one is given in appendix D. It is interesting to note that in the framework of electrical circuits, the forcing is directly seen as an input perturbation in temperature T_{eq} instead of a perturbation in radiative flux, from which the output temperature T can be derived by applying a transfer function $\mathcal{H}$. Indeed, these functions are apparent in the analytical solutions that are given in the following section.

APPENDIX B

General Solution of the Differential System

By rewriting in matrix form the set of coupled differential equations of the system [Eqs. (1) and (2)], one finds

$$\frac{d\mathbf{X}}{dt} = \mathbf{A}\mathbf{X} + \mathbf{B}, \tag{B1}$$

with

$$\mathbf{X}(t) = \begin{pmatrix} T \\ T_0 \end{pmatrix}, \quad \mathbf{A} = \begin{bmatrix} -(\lambda + \gamma)/C & \gamma/C \\ \gamma/C_0 & -\gamma/C_0 \end{bmatrix}, \quad \text{and}$$

$$\mathbf{B}(t) = \begin{pmatrix} \mathcal{F}/C \\ 0 \end{pmatrix}. \tag{B2}$$

The solution $\mathbf{X}^*$ of the homogeneous system ($\mathbf{B} = 0$) is given by

$$\mathbf{X}^*(t) = e^{t\mathbf{A}}\mathbf{X}(0). \tag{B3}$$

Yet, $\mathbf{A}$ can be factorized as $\mathbf{A} = \boldsymbol{\Phi}\mathbf{D}\boldsymbol{\Phi}^{-1}$, where $\mathbf{D}$ is the diagonal matrix whose diagonal elements are the eigenvalues of $\mathbf{A}$. One can show that

$$\mathbf{D} = \begin{pmatrix} -1/\tau_f & 0 \\ 0 & -1/\tau_s \end{pmatrix} \quad \text{and} \quad \boldsymbol{\Phi} = \begin{pmatrix} 1 & 1 \\ \phi_f & \phi_s \end{pmatrix}. \tag{B4}$$

The expression of τ_i and ϕ_i are given in Table 1. Since $e^{t\mathbf{A}} = \boldsymbol{\Phi}e^{t\mathbf{D}}\boldsymbol{\Phi}^{-1}$,

$$e^{t\mathbf{A}} = \boldsymbol{\Phi}\begin{pmatrix} e^{-t/\tau_f} & 0 \\ 0 & e^{-t/\tau_s} \end{pmatrix}\boldsymbol{\Phi}^{-1}, \tag{B5}$$

and the general solution of the homogeneous system is given by

$$T^*(t) = \frac{1}{\phi_s - \phi_f}(T_1 e^{-t/\tau_f} + T_2 e^{-t/\tau_s}) \quad \text{and} \tag{B6}$$

$$T_0^*(t) = \frac{1}{\phi_s - \phi_f}(\phi_f T_1 e^{-t/\tau_f} + \phi_s T_2 e^{-t/\tau_s}), \tag{B7}$$

with $T_1 = \phi_s T(0) - T_0(0)$ and $T_2 = -\phi_f T(0) + T_0(0)$.

To obtain the general solution of the nonhomogeneous system [$\mathbf{B}(t) \neq 0$], one can use the method known as *variation of parameter* by determining a particular solution of the form $\mathbf{X}(t) = e^{t\mathbf{A}}\mathbf{U}(t)$. By noting $\mathbf{U}'(t) = (e^{t\mathbf{A}})^{-1}\mathbf{B}(t)$, it is possible to derive the vector $\mathbf{U}$.

Finally, for any given forcing function $t \rightarrow \mathcal{F}(t)$, the general solution of the system (B1) is given by

$$T(t) = T^*(t) + \frac{1}{C(\phi_s - \phi_f)}\left[\phi_s \int_0^t \mathcal{F}(\xi)e^{-(t-\xi)/\tau_f}\,d\xi \right.$$
$$\left. - \phi_f \int_0^t \mathcal{F}(\xi)e^{-(t-\xi)/\tau_s}\,d\xi\right] \quad \text{and} \tag{B8}$$

$$T_0(t) = T_0^*(t) + \frac{\phi_s\phi_f}{C(\phi_s - \phi_f)}\left[\int_0^t \mathcal{F}(\xi)e^{-(t-\xi)/\tau_f}\,d\xi \right.$$
$$\left. - \int_0^t \mathcal{F}(\xi)e^{-(t-\xi)/\tau_s}\,d\xi\right]. \tag{B9}$$

Later on, we will consider $T(0) = 0$ and $T_0(0) = 0$. So, we have $T^*(t) = T_0^*(t) = 0$.

APPENDIX C

Stabilization and Abrupt Return to Preindustrial Forcing

a. Linearly increasing forcing and stabilization

The GFDL provided a simulation with a 1% yr^{-1} CO$_2$ increase up to a doubling of the atmospheric CO$_2$ concentration followed by a stabilization of this concentration at 2×CO$_2$. Such a simulation was also performed with the CNRM-CM5 climate model. These experiments are shown in Fig. 2. The corresponding analytical solution of the two-layer model is described hereafter.

In the case of a stabilization starting from time t_{st} of a 1% yr^{-1} CO$_2$ experiment,

$$\mathcal{F}(t) = \begin{cases} 0 & \text{if} \quad t < 0 \\ kt & \text{if} \quad 0 \le t < t_{st} \\ kt_{st} & \text{if} \quad t \ge t_{st}, \end{cases} \tag{C1}$$

the analytical solution for $0 \le t < t_{st}$ is the linear-forcing solution [Eqs. (14) and (15)]. For $t \ge t_{st}$, the solution is
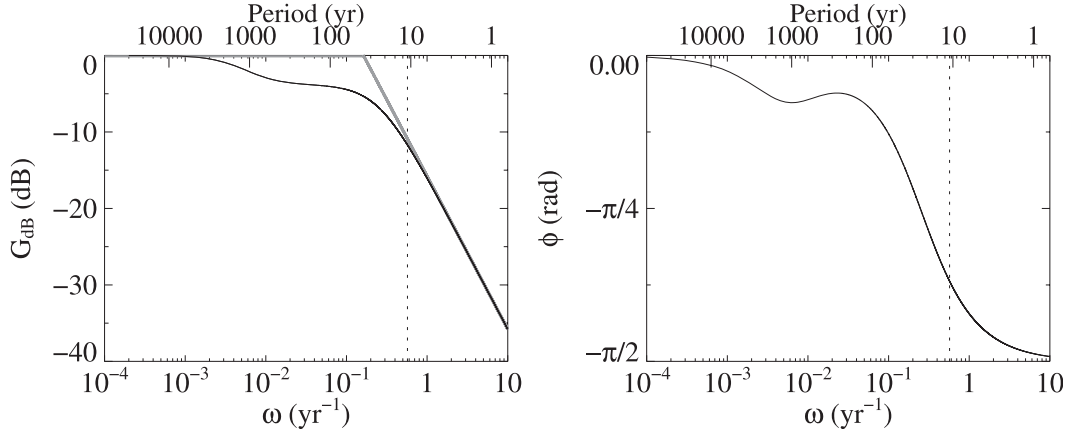
FIG. D1. Bode plot of the climate system in the framework of the two-layer energy-balance model with (left) gain G_{dB} in decibels and (right) phase Φ in radians. For the gain plot, the values of the asymptotes (gray lines) are given in the text. The vertical dotted lines indicate a periodic forcing of 11 yr. Values of gain and phase are for $\lambda = 1.3$ W m^{-2} K^{-1}, $C = 8$ W yr m^{-2} K^{-1}, $C_0 = 100$ W yr m^{-2} K^{-1}, and $\gamma = 0.7$ W m^{-2} K^{-1}.

$$T(t) = \frac{k}{\lambda}t_{st} - \frac{k}{\lambda}\sum_{i=\{s,f\}}\tau_i a_i[1 - e^{-(t_{st}/\tau_i)}]e^{-(t-t_{st})/\tau_i} \quad \text{and}$$

$$\text{(C2)}$$

$$T_0(t) = \frac{k}{\lambda}t_{st} - \frac{k}{\lambda}\sum_{i=\{s,f\}}\phi_i \tau_i a_i[1 - e^{-(t_{st}/\tau_i)}]e^{-(t-t_{st})/\tau_i}.$$

$$\text{(C3)}$$

b. Abrupt return to preindustrial (zero) forcing

Held et al. (2010) highlighted the interest of this case, showing that the slow response of the climate would maintain a significant climate perturbation, even if geoengineering was to provide a way to remove large amounts of CO_2 from the climate system. We hereafter describe the analytical solution corresponding to such abrupt return to preindustrial (zero) radiative forcing from a linear-forcing experiment.

In the case of an instantaneous return to preindustrial forcing at $t = t_{ar}$ from a linear-forcing transient regime,

$$\mathcal{F}(t) = \begin{cases} 0 & \text{if } t < 0 \\ kt & \text{if } 0 \le t < t_{ar}, \\ 0 & \text{if } t \ge t_{ar} \end{cases} \quad \text{(C4)}$$

the analytical solution for $t \ge t_{ar}$ is

$$T(t) = \frac{k}{\lambda}\sum_{i=\{s,f\}}\tau_i a_i\left[e^{-(t_{ar}/\tau_i)} - 1 + \frac{t_{ar}}{\tau_i}\right]e^{-(t-t_{ar})/\tau_i} \quad \text{and}$$

$$\text{(C5)}$$

$$T_0(t) = \frac{k}{\lambda}\sum_{i=\{s,f\}}\phi_i \tau_i a_i\left[e^{-(t_{ar}/\tau_i)} - 1 + \frac{t_{ar}}{\tau_i}\right]e^{-(t-t_{ar})/\tau_i}.$$

$$\text{(C6)}$$

When neglecting the fast term, the remaining term, which slowly tends to zero, is the *recalcitrant* component of global warming (Held et al. 2010).

APPENDIX D

Periodic Forcing

The two-layer EBM can be used to understand not only long-term climate trends caused by CO_2, but also to study climate perturbations caused by other radiative perturbations (such as perturbations of the solar forcing), and even climate variability resulting from the variability of the radiative forcing. As an example, we hereafter give the analytical solution of the two-layer EBM response to a periodic forcing, that could be used to understand the climate variability associated with the natural solar variability.

In a stationary regime, the solution of a periodic forcing $\mathcal{F}(t) = \mathcal{F}e^{i\omega t}$ is

$$T(t) = \frac{C_0 i\omega + \gamma}{(Ci\omega + \lambda + \gamma)(C_0 i\omega + \gamma) - \gamma^2}\mathcal{F}(t) \quad \text{and} \quad \text{(D1)}$$

$$T_0(t) = \frac{\gamma}{(Ci\omega + \lambda + \gamma)(C_0 i\omega + \gamma) - \gamma^2}\mathcal{F}(t). \quad \text{(D2)}$$

Thus the transfer function $\mathcal{H}$ of the system is

$$\mathcal{H}(i\omega) = \frac{T(t)}{T_{eq}(t)} = \left(\frac{a_f}{1 + i\omega\tau_f} + \frac{a_s}{1 + i\omega\tau_s} \right). \quad (D3)$$

We can also write the transfer function in a canonical form

$$\mathcal{H}(i\omega) = \frac{1 + i\dfrac{\omega}{\omega_1}}{\dfrac{(i\omega)^2}{\omega_0^2} + 2\xi\dfrac{i\omega}{\omega_0} + 1}, \quad (D4)$$

by noting $\omega_1 = 1/(a_f\tau_s + a_s\tau_f)$, $\omega_0 = 1/\sqrt{\tau_f\tau_s}$, and $\xi = (\tau_f + \tau_s)/(2\sqrt{\tau_f\tau_s})$.

By using the notation $\overline{\omega} = \omega/\omega_0$, the gain G of the system is given by

$$G(\omega) = |\mathcal{H}(i\omega)| = \frac{\sqrt{1 + (\omega/\omega_1)^2}}{\sqrt{(1 - \overline{\omega}^2)^2 + (2\xi\overline{\omega})^2}}. \quad (D5)$$

Also, the phase Φ is

$$\Phi(\omega) = \arctan\left(\frac{\omega}{\omega_1}\right) + \arctan\left(\frac{2\xi\overline{\omega}}{\overline{\omega}^2 - 1}\right). \quad (D6)$$

The Bode plot that shows $G_{dB}(\omega) = 20\log G(\omega)$ and $\Phi(\omega)$ against $\log\omega$ is represented in Fig. D1. Asymptotically, we have

$$G_{dB}(\omega \to 0) = 0 \quad \text{and} \quad (D7)$$

$$G_{dB}(\omega \to \infty) = -20\log\omega + 20\log(\omega_c), \quad (D8)$$

with a cutoff frequency

$$\omega_c = \omega_0^2/\omega_1 = \frac{\lambda}{C}. \quad (D9)$$

For the 11-yr solar cycle, with $\lambda = 1.3$ W m^{-2} K^{-1}, $C = 8$ W yr m^{-2} K^{-1}, $C_0 = 100$ W yr m^{-2} K^{-1}, and $\gamma = 0.7$ W m^{-2} K^{-1}, the amplitude of the response is attenuated by approximately 10 dB and is shifted by about 4 yr.

REFERENCES

Andrews, T., J. M. Gregory, M. J. Webb, and K. E. Taylor, 2012: Forcing, feedbacks and climate sensitivity in CMIP5 coupled atmosphere–ocean climate models. *Geophys. Res. Lett.,* **39,** L09712, doi:10.1029/2012GL051607.

Budyko, M. I., 1969: The effect of solar radiation variations on the climate of the Earth. *Tellus,* **5,** 611–619.

Dickinson, R., 1981: Convergence rate and stability of ocean–atmosphere coupling schemes with a zero-dimensional climate model. *J. Atmos. Sci.,* **38,** 2112–2120.

Dufresne, J.-L., and S. Bony, 2008: An assessment of the primary sources of spread of global warming estimates from coupled atmosphere–ocean models. *J. Atmos. Sci.,* **21,** 5135–5144.

Friend, A. D., 2011: Response of Earth's surface temperature to radiative forcing over A.D. 1–2009. *J. Geophys. Res.,* **116,** D13112, doi:10.1029/2010JD015143.

Geoffroy, O., D. Saint-Martin, G. Bellon, A. Voldoire, D. J. L. Olivié, and S. Tytéca, 2013: Transient climate response in a two-layer energy-balance model. Part II: Representation of the efficacy of deep-ocean heat uptake and validation for CMIP5 AOGCMs. *J. Climate,* **26,** 1859–1876.

Good, P., J. M. Gregory, and J. A. Lowe, 2011: A step-response simple climate model to reconstruct and interpret AOGCM projections. *Geophys. Res. Lett.,* **38,** L01703, doi:10.1029/2010GL045208.

Gregory, J. M., 2000: Vertical heat transports in the ocean and their effect on time-dependent climate change. *Climate Dyn.,* **16,** 505–515.

——, and J. F. B. Mitchell, 1997: The climate response to CO_2 of the Hadley Centre coupled AOGCM with and without flux adjustment. *Geophys. Res. Lett.,* **24,** 1943–1946.

—— and P. M. Forster, 2008: Transient climate response estimated from radiative forcing and observed temperature change. *J. Geophys. Res.,* **113,** D23105, doi:10.1029/2008JD010405.

——, and M. Webb, 2008: Tropospheric adjustment induces a cloud component in CO_2 forcing. *J. Climate,* **21,** 58–71.

——, and Coauthors, 2004: A new method for diagnosing radiative forcing and climate sensitivity. *Geophys. Res. Lett.,* **31,** L03205, doi:10.1029/2003GL018747.

Hansen, J., and Coauthors, 2005: Efficacy of climate forcings. *J. Geophys. Res.,* **110,** D18104, doi:10.1029/2005JD005776.

Hasselmann, K., R. Sausen, E. Maier-Reimer, and R. Voss, 1993: On the cold start problem in transient simulations with coupled atmosphere–ocean models. *Climate Dyn.,* **9,** 53–61.

Held, I. M., M. Winton, K. Takahashi, T. Delworth, F. Zeng, and G. K. Vallis, 2010: Probing the fast and slow components of global warming by returning abruptly to preindustrial forcing. *J. Climate,* **23,** 2418–2427.

Houghton, J. T., G. J. Jenkins, and J. J. Ephraums, Eds., 1990: *Climate Change: The IPCC Scientific Assessment.* Cambridge University Press, 410 pp.

Meinshausen, M., S. C. B. Raper, and T. M. L. Wigley, 2011: Emulating coupled atmosphere–ocean and carbon cycle models with a simpler model, MAGICC6—Part 1: Model description and calibration. *Atmos. Chem. Phys.,* **11,** 1417–1456.

Murphy, J. M., 1995: Transient response of the Hadley Centre coupled ocean–atmosphere model to increasing carbon dioxide. Part III: Analysis of global-mean response using simple models. *J. Climate,* **8,** 496–514.

Olivié, D. J. L., G. P. Peters, and D. Saint-Martin, 2012: Atmosphere response time scales estimated from AOGCM experiments. *J. Climate,* **25,** 7956–7972.

Plattner, G. K., and Coauthors, 2008: Long-term climate commitments projected with climate–carbon cycle models. *J. Climate,* **21,** 2721–2751.

Raper, S. C. B., J. M. Gregory, and R. J. Stouffer, 2002: The role of climate sensitivity and ocean heat uptake on AOGCM transient temperature response. *J. Climate,* **15,** 124–130.

Schwartz, S. E., 2008: Reply to comments by G. Foster et al., R. Knutti et al., and N. Scafetta on "Heat capacity, time constant, and sensitivity of Earth's climate system." *J. Geophys. Res.,* **113,** D15105, doi:10.1029/2008JD009872.

Sellers, W. D., 1969: A global climatic model based on the energy balance of the earth–atmosphere system. *J. Appl. Meteor.,* **8,** 392–400.

Soden, B. J., and I. M. Held, 2006: An assessment of climate feedbacks in coupled ocean–atmosphere models. *J. Climate,* **19,** 3354–3360.

Taylor, K. E., R. J. Stouffer, and G. A. Meehl, 2011: An overview of CMIP5 and the experiment design. *Bull. Amer. Meteor. Soc.,* **93,** 485–498.

van Hateren, J. H., 2013: A fractal climate response function can simulate global average temperature trends of the modern era and the past millennium. *Climate Dyn.,* doi:10.1007/s00382-012-1375-3, in press.

Williams, K. D., W. J. Ingram, and J. M. Gregory, 2008: Time variation of effective climate sensitivity in GCMs. *J. Climate,* **21,** 5076–5090.

Winton, M., K. Takahashi, and I. M. Held, 2010: Importance of ocean heat uptake efficacy to transient climate change. *J. Climate,* **23,** 2333–2344.